Assessment of transition metal-doped Zinc Oxide nanoparticle for ions trapping: bridging structural and electronic insights by DFT optimization

Fatemeh Mollaamin*

Department of Biomedical Engineering, Faculty of Engineering and Architecture, Kastamonu University, Kastamonu, Turkey

*Corresponding Author:
email*: fmollaamin@kastamonu.edu.tr

Received: April 21, 2026
Accepted: Mei 29, 2026

DOI: 10.1980/jses.v1i1.15

Phone*: +905521529037

Abstract: *A detailed study was performed using "DFT" calculations at the "CAM-B3LYP-D3/6-311+G (d,p)" level to investigate how H_2O is captured by a ZnO, ZnTiO, ZnCrO, ZnMnO or ZnNiO heterocluster. The weak signal strength observed near the parallel edge of the nanocluster sample could be because of the non-spherical arrangement of these heteroclusters caused by H/OH binding. This hypothesis about energy absorption was supported by analyzing the density distributions of "TDOS, PDOS, OPDOS, LOL" for water-coated ZnO, ZnTiO, ZnCrO, ZnMnO and ZnNiO heteroclusters. An isosurface map showed a larger area involved in H_2O adsorption on the surface, leading to the formation of hydrated complexes of ZnO-(H^+OH^-), ZnTiO-(H^+OH^-), ZnCrO-(H^+OH^-), ZnMnO-(H^+OH^-) and ZnNiO-(H^+OH^-) with specific atoms labeled as "O1, Zn/Ti/Cr/Mn/Ni, O27, H29, and H30". Based on this, it could be said that the Zn/Ti/Cr/Mn/Ni in the cubic heteroclusters, respectively has a greater ability to accept electrons during H_2O adsorption. It's also important to note that when all the surface elements of these heteroclusters are covered by "OH^-/H^+" ions, the semiconducting treatment is restored. These findings suggest that the electronic properties can be adjusted by controlling the adsorption position on the surface. The findings can potentially lead to the development of more efficient water purification processes through further research on photocatalysts.*

Keywords: *ZnTiO, ZnCrO, ZnMnO, ZnNiO, semiconducting heterocluster, H_2O-adsorption, first-principles study*

Introduction

ZnO is a great semiconductor material that can be used in many different areas like optoelectronics and biomedicine. This is because it has a wide direct band gap, a high exciton binding energy, good electron mobility, and high quantum efficiency. To enhance the performance of ZnO devices, plasma treatment is often used to modify the surface [1–4]. This treatment changes the luminescence characteristics of ZnO, affecting ultraviolet (UV) luminescence, visible light emission, and the recombination process [5–11]. Using H plasma greatly improves optical properties without changing the thickness much. Even though no chemical reactions happen, Ar plasma boosts emission intensity by removing areas where light is lost through non-radiative recombination. Both H and Ar plasma also cause strong exciton localization, which results in a much broader UV spectrum [12–15].

However, it is often difficult to replicate or apply the reported improvements in plasma treatments for ZnO. This challenge comes from several reasons. First, ZnO samples can have different properties such as thin films, single crystals, or nanostructures made using various methods. Also, the specific effects of plasma treatments with different gases are not well understood, since each gas plasma behaves differently. Because of this, it is important to carefully compare how different plasma gases affect the optical and electrical properties of ZnO and to clearly identify which specific defects are involved [16–21]. Transparent and highly water-attracting materials are very important because of their ability to clean themselves, which has become a widely studied area, especially in solar panel technology. Some research has shown that by changing the shape of zinc oxide, both hydrophilic and superhydrophilic forms can be created, making them useful as self-cleaning coatings for solar panels [22].

The researchers used molecular dynamics simulations with a reactive force-field to study the ZnO-H_2O system under normal conditions. The force-field parameters were adjusted based on data from density functional theory calculations, which included energy levels, molecular shapes, and charge distributions. The model they developed matched well with the quantum mechanics data from the dataset. They used this model to examine how water molecules attach to ZnO surfaces, either as whole molecules or broken apart, at different temperatures. The surfaces studied included both flat and stepped structures. The findings indicate that structures that support hydrogen bonding are more favorable, and the presence of steps leads to a higher degree of hydroxylation in the water layers [23].

In recent years, semimagnetic semiconductors have gained a lot of attention due to their wide range of useful properties in spintronics applications. These materials are usually created by adding a small amount of transition metals, such as Fe, Co, Ni, Ti, Cr, and others, into semiconductor materials [24]. Recently, scientists managed to create Ti-doped ZnO nanoparticles using the co-precipitation method. A vibrating sample magnetometer showed that pure ZnO and Ti-doped ZnO both showed ferromagnetic properties at room temperature [25]. Among transition metals, titanium can be easily replaced by host ions because its d subshells are only partially filled [26]. In addition, the effect of doping Cr ions on the structure, optical, and magnetic properties of ZnO was studied. Photoluminescence and electron paramagnetic resonance showed the presence of negatively charged zinc vacancies and singly ionized oxygen vacancies in ZnO. The long-range ferromagnetic ordering observed was explained using the bound magnetic polaron mechanism [27].

Recently, pure and manganese doped zinc oxide nanoparticles have been successfully synthesized by a solution growth process. The effect of Mn doping on the structure, morphology and optical properties was investigated by several techniques. The optical band gap of the ZnO nanoparticles decreased linearly with increasing Mn percent doping, suggesting the possibility of tuning the band gap of ZnO by doping with Mn [28]. Furthermore, Ni-doped ZnO nanoparticles were synthesized through a simple chemical growth route using hydroxyoxalate type materials. The excitonic peaks observed from absorption spectra of the prepared nanoparticles exhibit blue shift for nickel doping [29].

In this study, we looked at how H_2O adsorption affects the properties of a ZnO, ZnTiO, ZnCrO, ZnMnO or ZnNiO nanocluster. It was used DFT calculations to examine the density of states, charge distribution, bond orders, and HOMO-LUMO orbitals. The optimized structures of ZnTiO-(H^+OH^-), ZnCrO-(H^+OH^-), ZnMnO-(H^+OH^-) and ZnNiO-(H^+OH^-) have been shown in Figure 1, and the zinc/titanium/chromium/manganese/nickel, oxygen and hydrogen atoms are labeled to help explain the reaction pathway.

In this study, ZnO-(H^+OH^-), ZnTiO-(H^+OH^-), ZnCrO-(H^+OH^-), ZnMnO-(H^+OH^-) or ZnNiO-(H^+OH^-) sensor was successfully used to detect relative humidity through nearest neighbor analysis. The way water molecules attach to the surface of ZnO, ZnTiO, ZnCrO, ZnMnO or ZnNiO was also studied using density functional theory.

Method

Improvement of the applied Density Functional Theory (DFT) methodology only became notable after W. Kohn and L. J. Sham released their reputable series of equations which are introduced as Kohn-Sham (KS) equations [30,31]:

$$\hat{H}_s = -\sum_i^M \frac{1}{2} \overline{\nabla}_i^2 + \sum_i^M v_s(\vec{r}_i) = \sum_i^M \hat{h}_s \quad (1)$$

$$\hat{h}_s = -\frac{1}{2} \overline{\nabla}_i^2 + v_s(\vec{r}_i) \quad (2)$$

By representing the single particle orbitals ψ_i all electronic densities physically acceptable for the system of "non-interacting" electrons are written in the equation (3):

$$\rho(\vec{r}) = \sum_i^M |\psi_i(\vec{r})|^2 \quad (3)$$

Finally, the total energy could be measured by the KS method due to the equation (4):

$$E[\rho] = T_s[\rho] + \int dr \; v_{ext}(r)\rho(r) + E_{\mathrm{H}}[\rho] + E_{\mathrm{xc}}[\rho] \quad (4)$$

where kinetic energy functional, v_{ext} declares external potential, E_{H} is the "Hartree or Coulomb" energy and E_{xc} indicates exchange-correlation functional. Therefore, the precise exchange energy functional is described by the Kohn–Sham orbitals in lieu of the density which is cited as the indirect density functional.

This research has employed the penetration of the hybrid functional of three-parameter basis set of B3LYP (Becke, Lee, Yang, Parr)" within the conception of DFT upon theoretical computations [31]. The popular B3LYP (Becke, three-parameter, Lee–Yang–Parr) and exchange-correlation functional becomes based on equation (5) [32]:

$$E_{XC}^{B3LYP} = (1-\alpha)E_x^{LSDA} + \alpha E_x^{HF} + b\Delta E_x^{B} + (1-c)E_c^{LSDA} + cE_c^{LYP} \quad (5)$$

Calculations with spin polarization were performed within the "density functional theory (DFT)". The exchange correlation potentials were treated using the "Perdew–Burke–Ernzerhof (PBE)" parameterization within the "general gradient approximation (GGA)" [33].

The hydration of bare ZnO, ZnTiO, ZnCrO, ZnMnO or ZnNiO heterocluster and the formation of the hydrated" ZnO-(H^+OH^-), ZnTiO-(H^+OH^-), ZnCrO-(H^+OH^-), ZnMnO-(H^+OH^-) or ZnNiO-(H^+OH^-)" heterocluster were studied using quantum mechanics computations based on "density functional theory (DFT)" (Figure 1) [34,35]. A "rigid potential energy surface" was calculated using "DFT" [36,37] with the "Gaussian 16 revision C.01 program package" [38] and "GaussView 6.1" [39]. The calculations used the "6-311+G(d,p)" basis set for energy storage applications in solar cells.

The structural settings of the ZnO, ZnTiO, ZnCrO, ZnMnO or ZnNiO heterocluster and the hydrated nanocluster of ZnO-(H^+OH^-), ZnTiO-(H^+OH^-), ZnCrO-(H^+OH^-), ZnMnO-(H^+OH^-) or ZnNiO-(H^+OH^-), respectively, were adjusted to achieve the highest possible "short-circuit" current density (Figure 1).

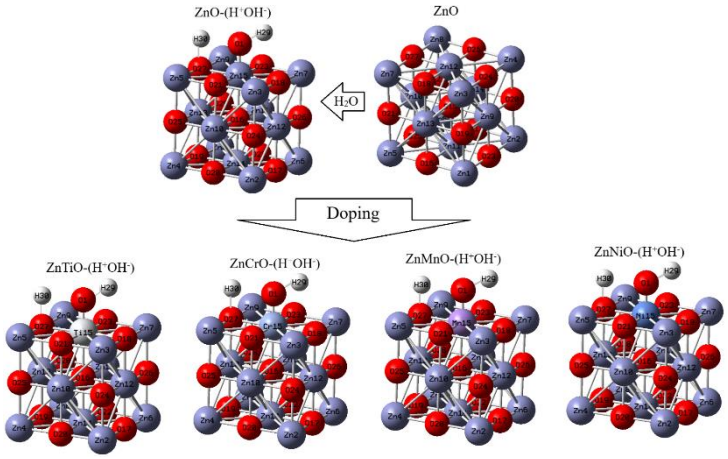

Figure 1. Functionalization of bare ZnO and ZnO (H^+OH^-) through formation of transition metal doped complexes of ZnTiO-(H^+OH^-), ZnCrO-(H^+OH^-), ZnMnO-(H^+OH^-) and ZnNiO-(H^+OH^-) using a labeled ring in a clockwise direction, showing H, O, Zn, Ti, Cr, Mn, Ni atoms involved in H_2O adsorption.

Result and Discussion

In this article, the data assesses how effective ZnO, ZnTiO, ZnCrO, ZnMnO or ZnNiO heterocluster is in water using information about energy, shape, and charge obtained from "density functional theory" computations. The sample used matches well with quantum mechanics data for the hydrated ZnO-(H^+OH^-), ZnTiO-(H^+OH^-), ZnCrO-(H^+OH^-), ZnMnO-(H^+OH^-) or ZnNiO-(H^+OH^-) system found in the "dataset". Additionally, the atomic charge was examined during the adsorption of H_2O on ZnO, ZnTiO, ZnCrO, ZnMnO or ZnNiO nanocluster, which contributed to the formation of ZnO-(H^+OH^-), ZnTiO-(H^+OH^-), ZnCrO-(H^+OH^-), ZnMnO-(H^+OH^-) or ZnNiO-(H^+OH^-) complex (Table 1).

The atomic charges of "zinc, titanium, chromium, manganese, nickel, oxygen, and hydrogen or hydroxyl groups" attached to ZnO, ZnTiO, ZnCrO, ZnMnO or ZnNiO have been measured. These measurements show that when water is added, the negative charge on oxygen atoms in the "O16 to O28" region of "hydrated complexes "changes due to the coating of them with H or OH" groups (Table 1 and Figure 2).

Table 1. The "atomic charge (Q/coulomb)" for "hydrated heteroclusters of ZnO(H^+OH^-), ZnTiO-(H^+OH^-), ZnCrO-(H^+OH^-), ZnMnO-(H^+OH^-), and ZnNiO-(H^+OH^-)".

ZnO-(H^+OH^-)		ZnTiO-(H^+OH^-)		ZnCrO-(H^+OH^-)		ZnMnO-(H^+OH^-)		ZnNiO-(H^+OH^-)	
A	Q	A	Q	A	Q	A	Q	A	Q
O1	–0.59	Zn1	0.21	Zn1	0.14	Zn1	–0.02	Zn1	–0.41
Zn2	0.69	Zn2	0.74	Zn2	0.71	Zn2	0.67	Zn2	0.69
Zn3	0.73	Zn3	0.64	Zn3	0.61	Zn3	0.61	Zn3	0.69
Zn4	0.72	Zn4	0.73	Zn4	0.72	Zn4	0.70	Zn4	0.72
Zn5	0.59	Zn5	0.54	Zn5	0.60	Zn5	0.53	Zn5	0.65
Zn6	0.69	Zn6	0.74	Zn6	0.71	Zn6	0.67	Zn6	0.69
Zn7	0.71	Zn7	0.63	Zn7	0.60	Zn7	0.60	Zn7	0.67
Zn8	0.72	Zn8	0.73	Zn8	0.72	Zn8	0.70	Zn8	0.71
Zn9	0.60	Zn9	0.54	Zn9	0.60	Zn9	0.52	Zn9	0.65
Zn10	1.72	Zn10	1.63	Zn10	1.68	Zn10	1.80	Zn10	1.81
Zn11	1.73	Zn11	1.63	Zn11	1.69	Zn11	1.80	Zn11	1.81
Zn12	1.88	Zn12	1.95	Zn12	1.93	Zn12	1.91	Zn12	1.94
Zn13	1.90	Zn13	1.94	Zn13	1.82	Zn13	1.88	Zn13	2.04
Zn14	1.70	Zn14	1.84	Zn14	1.83	Zn14	1.80	Zn14	1.74
Zn15	1.48	Ti15	0.31	Cr15	0.00	Mn15	–0.05	Ni15	–0.06
O16	–1.54	O16	–1.44	O16	–1.44	O16	–1.45	O16	–1.46
O17	–1.22	O17	–1.22	O17	–1.22	O17	–1.22	O17	–1.22
O18	–1.21	O18	–1.01	O18	–0.93	O18	–0.91	O18	–0.99
O19	–1.22	O19	–1.22	O19	–1.22	O19	–1.22	O19	–1.22
O20	–1.22	O20	–1.22	O20	–1.22	O20	–1.22	O20	–1.22
O21	–1.14	O21	–1.05	O21	–0.93	O21	–0.87	O21	–0.96
O22	–1.22	O22	–1.22	O22	–1.22	O22	–1.22	O22	–1.22
O23	–1.13	O23	–1.05	O23	–0.92	O23	–0.87	O23	–0.96
O24	–1.21	O24	–1.22	O24	–1.22	O24	–1.22	O24	–1.22
O25	–1.22	O25	–1.22	O25	–1.22	O25	–1.23	O25	–1.22
O26	–1.21	O26	–1.22	O26	–1.22	O26	–1.22	O26	–1.22
O27	–1.18	O27	–0.97	O27	–0.93	O27	–0.89	O27	–1.00
O28	–1.22	O28	–1.22	O28	–1.22	O28	–1.23	O28	–1.22
H29	0.29	H29	0.19	H29	0.23	H29	0.28	H29	0.39
H30	0.37	H30	0.28	H30	0.31	H30	0.37	H30	0.37

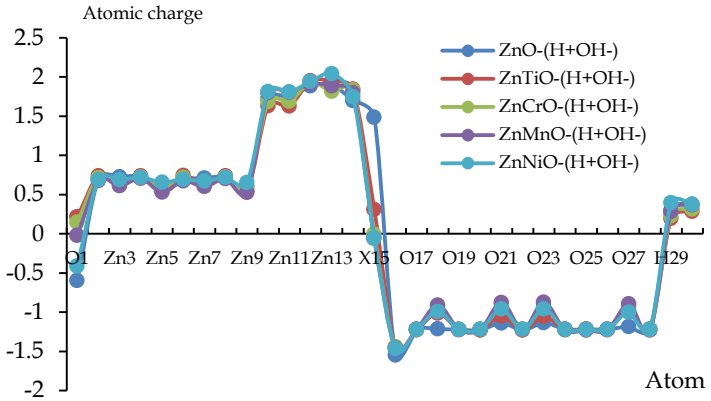

Figure 2. "Atomic charge (Q/coulomb)" for atoms in "ZnO-(H^+OH^-), ZnTiO-(H^+OH^-), ZnCrO-(H^+OH^-), ZnMnO-(H^+OH^-), and ZnNiO-(H^+OH^-)". (Note: X= Zn, Ti, Cr, Mn or Ni)

Water mainly attaches to the surface of ZnO, ZnTiO, ZnCrO, ZnMnO or ZnNiO nanoparticles by forming Zn-O, Ti-O, Cr-O, Mn-O, or Ni-O bond. Compared to bulk ZnO crystals, ZnTiO, ZnCrO, ZnMnO or ZnNiO nanoparticle can hold more water molecules per unit surface area because their curved structure increases the distance between neighboring water molecules (Figure 2).

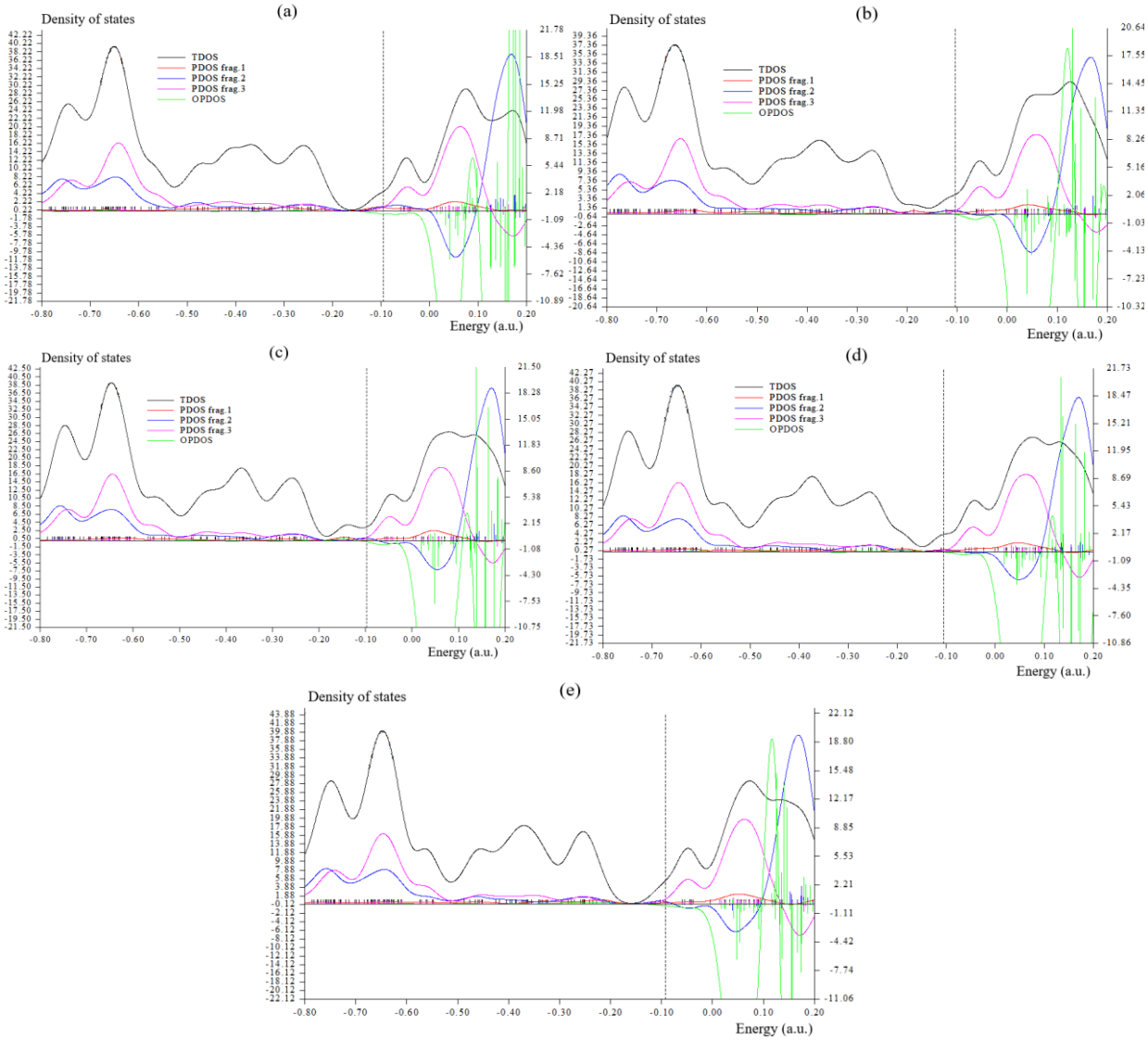

Figure 3. The "TDOS/PDOS/OPDOS" graphs for heteroclusters of (a) ZnO-(H^+OH^-), (b) ZnTiO-(H^+OH^-), (c) ZnCrO-(H^+OH^-), (d) ZnMnO-(H^+OH^-), and (e) ZnNiO-(H^+OH^-).

To better understand the different adsorption behaviors of bare heteroclusters of "ZnO, ZnTiO, ZnCrO, ZnMnO or ZnNiO " and hydrated complexes of " ZnO-(H^+OH^-), ZnTiO-(H^+OH^-), ZnCrO-(H^+OH^-), ZnMnO-(H^+OH^-) and ZnNiO-(H^+OH^-)", "total density of states (TDOS)" [40] was calculated using the Multiwfn program [41,42]. This parameter helps identify "significant chemical interactions", often occurring on the "convex side" (Figure 3a–e). Therefore, the original total "DOS (TDOS)" of the "isolated system" can be expressed as [40]:

$$TDOS\ (E) = \sum_i \delta\ (E - \epsilon_i\ ) \quad (6)$$

$$G(x) = \frac{1}{c\sqrt{2\pi}} e^{-\frac{x^2}{2c^2}}$$

$$\text{where}\quad c = \frac{\text{FWHM}}{2\sqrt{2\ln x}} \quad (7)$$

In addition, the curve map of "broadened partial DOS (PDOS)" and overlap "DOS (OPDOS)" is useful for visualizing the "orbital composition" analysis, and the "PDOS function of fragment" "*A*" is defined as:

$$PDOS_A\ (E) = \sum_i \Xi_{i,A}\ F\ (E - \epsilon_i\ ) \quad (8)$$

where "$\Xi_{i,A}$" is the "composition of fragment" "*A*" in orbital "*i*". The OPDOS between fragment "*A*" and "*B*" is defined as:

$$OPDOS_{A,B}\ (E) = \sum_i \mathrm{X}^i_{A,B}\ F\ (E - \epsilon_i\ ) \quad (9)$$

Where "$\mathrm{X}^i_{A,B}$" describes "the total cross term between fragments" "*A*" and "*B*" in orbital "i ". In the "TDOS map", "each vertical line" declares a "molecular orbital (MO) ", and the "dashed line" shows the position of the "HOMO". The curve shows the "TDOS"

computed based on the energy distribution of the molecular orbitals. Our findings suggest that electronic properties can be tailored by adjusting the "surface adsorption sites". In the positive energy range, the area between 0.1 to 0.2 a.u. shows a significantly higher state density compared to other regions for bare heteroclusters of "ZnO, ZnTiO, ZnCrO, ZnMnO or ZnNiO" and hydrated complexes of " ZnO-(H^+OH^-), ZnTiO-(H^+OH^-), ZnCrO-(H^+OH^-), ZnMnO-(H^+OH^-) and ZnNiO-(H^+OH)" (Figure 3a–e).

Fragment 1 includes O1, Zn2, Zn4, Zn6, Zn8, Zn10, O16, O19, O22, O24 along with H30 (Figure 3a). Fragment 2 shows the movement of Zn11, Zn12, Zn13, Zn14, O17, O25, O26, O27 and H29 for ZnO-(H^+OH^-), ZnTiO-(H^+OH^-), ZnCrO-(H^+OH^-), ZnMnO-(H^+OH^-) or ZnNiO-(H^+OH^-) complex (Figure 3b–e). Fragment 3 includes the movement of "Zn3, Zn5, Zn7, Zn9, O18, O20, O21, O23" for hydrated complexes (Figure 3b–e).

The "Localized Orbital Locator (LOL) " has a similar expression to the "Electron Localization Function (ELF) " [43].

$$\mathrm{LOL}(\mathbf{r}) = \frac{\tau(\mathbf{r})}{1+\tau(\mathbf{r})};\tau(\mathbf{r}) = \frac{D_0(\mathbf{r})}{\frac{1}{2}\sum_i \eta_i|\nabla\varphi_i(\mathbf{r})|^2} \quad (10)$$

$$D_0(\mathbf{r}) = \frac{3}{10}(6\pi^2)^{2/3}\left[\rho_\alpha(\mathbf{r})^{5/3} + \rho_\beta(\mathbf{r})^{5/3}\right] \quad (11)$$

"Multiwfn" [41,42] also supports a version of "LOL" developed by "Tsirelson and Stash" [44]. In this version, the kinetic energy part of "LOL" is replaced with a "second-order gradient" expansion, similar to how "ELF" works. This method can handle a wide variety of bonding situations. To use this version of LOL, you need to set "ELFLOL_type" to 1 in the settings. For specific reasons, if you change "ELFLOL_type" from 0 to 2 in settings.ini, a different approach will be applied.

$$\mathrm{LOL}(\mathbf{r}) = \frac{1}{1+\left[1/\tau(\mathbf{r})\right]^2} \quad (12)$$

If the "ELFLOL_cut" parameter in "settings.ini" is set to a certain value "x", then "LOL" will be "zero" for any case where "LOL" is less than x.

The hydrated ZnO, ZnTiO, ZnCrO, ZnMnO or ZnNiO heterocluster can be identified using LOL graphs, as they help in understanding the delocalization and localization of "electrons and chemical bonds" (Figure 4 a–e).

"Covalent zones" have a "high LOL value", and the areas where electrons are missing between the "valence shell" and the inner shell are shown by the "blue circles around the nuclei" (Figure 4a–e). The shaded map of LOL for bare and hydrated ZnO, ZnTiO, ZnCrO, ZnMnO or ZnNiO heterocluster (Figure 4a–e) shows how the "localized orbital locator" changes with "H/OH adsorption". The hydrated heterocluster of "ZnO-(H^+OH^-), ZnTiO-(H^+OH), ZnCrO-(H^+OH^-), ZnMnO-(H^+OH^-) and ZnNiO-(H^+OH^-) " has a larger "isosurface map" of the "localized orbital locator" because it labels specific atoms like "O1, Zn15/Ti15/Cr15/Mn15/ Ni15, O27, H29, and H30". A narrower connected area in the "isosurface map" suggests that the "localized orbital locator" is harder to achieve. However, the bigger "counter map" of LOL for hydrated heterocluster of " ZnO-(H^+OH^-), ZnTiO-(H^+OH^-), ZnCrO-(H^+OH^-), ZnMnO-(H^+OH^-) or ZnNiO-(H^+OH^-) " shows that these heteroclusters could be a great semiconductor material for many uses.

In addition, the overlap between molecular orbitals plays a key role in understanding how charge moves between molecules. This includes calculating the overlap between the "highest occupied molecular orbitals (HOMO)" and the "lowest unoccupied molecular orbitals (LUMO)" in the H/OH group and the ZnO, ZnTiO, ZnCrO, ZnMnO or ZnNiO heterocluster. The calculation uses the "CAM-B3LYP-D3/6-311+G (d,p)" wavefunction level, which is used to determine the HOMO and LUMO values, respectively (see Table 2).

As water molecules approach the surface, their shape and electric charge arrangement undergo a significant change. This phenomenon is enhanced by the presence of a metal atom such as titanium or chromium on the ZnO surface, which increases the polarity of the water molecules. Consequently, the electric charge arrangement of water molecules at the surface is more pronounced compared to when they are isolated (Table 2). Comparing the undoped ZnO nanoparticles and the Ni-doped ZnO nanoparticle showed that Ni ions replaced Zn ions effectively.

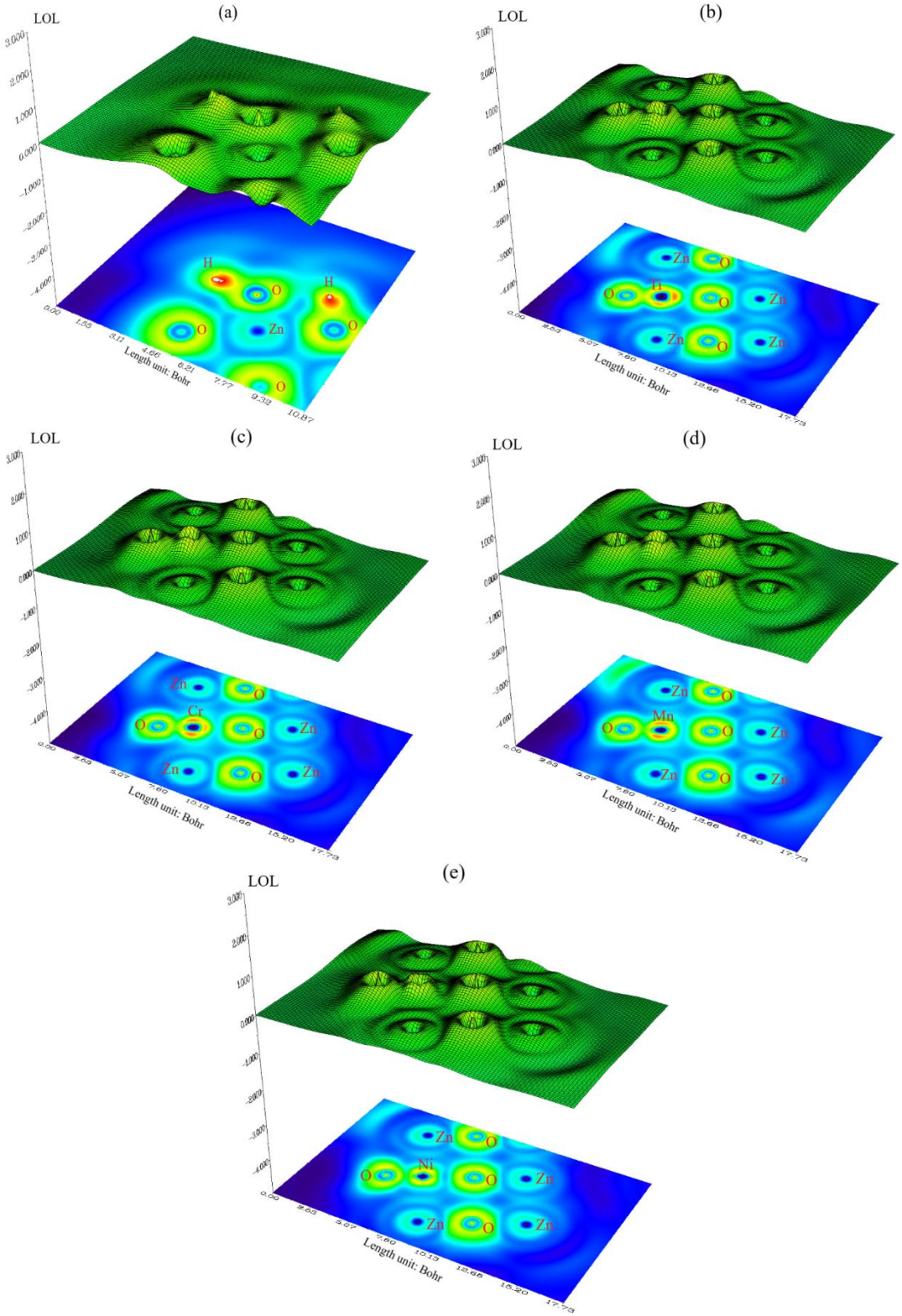

Figure 4. Counter map graphs of the localized orbital locator (LOL) for heteroclusters of (a) ZnO-(H^+OH^-), (b) ZnTiO-(H^+OH^-), (c) ZnCrO-(H^+OH^-), (d) ZnMnO-(H^+OH^-), and (e) ZnNiO-(H^+OH^-), plotted against length unit in Bohr.

Table 2. Stability energy (E_s, kcal/mol), dipole moment (D, debye), LUMO (eV), HOMO(eV), and energy gap (ΔE, eV) for heteroclusters of bare ZnO and hydrated ones of ZnO-(H^+OH^-), ZnTiO-(H^+OH^-), ZnCrO-(H^+OH^-), ZnMnO-(H^+OH^-) or ZnNiO-(H^+OH).

Heteroclusters	$E_s \times 10^{-6}$ (kcal/mol)	D (debye)	E_{HOMO} (eV)	E_{LUMO} (eV)	ΔE= E_{LUMO} – E_{HOMO} (eV)
ZnO	–1.18	0.00	–2.43	–1.30	1.12
ZnO(H^+OH^-)	–1.23	3.95	–2.61	–1.60	1.00
ZnTiO-(H^+OH^-)	–1.22	5.14	–2.81	–1.69	1.12
ZnCrO-(H^+OH^-)	–1.24	4.35	–2.67	–1.60	1.06
ZnMnO-(H^+OH^-)	–1.25	4.80	–2.97	–1.91	1.05
ZnNiO-(H^+OH^-)	–1.29	3.97	–2.51	–1.63	o.87

Conclusion

It's important to understand how water interacts with ZnO, ZnTiO, ZnCrO, ZnMnO or ZnNiO heterocluster because this knowledge is crucial for using the material in areas like gas sensing, catalysis, and biomedical uses. The hydrated ZnO-(H^+OH^-), ZnTiO-(H^+OH^-), ZnCrO-(H^+OH^-), ZnMnO-(H^+OH^-) or ZnNiO-(H^+OH^-) heterocluster shows a bigger electron delocalization area because of the labeled atoms "O1, Zn15/ Ti15/Cr15/Mn15/ Ni15, O27, H29, and H30". A smaller connected area in the "isosurface map" suggests that "electron delocalization" is harder to achieve. However, the larger LOL map for hydrated ZnO-(H^+OH^-), ZnTiO-(H^+OH^-), ZnCrO-(H^+OH^-), ZnMnO-(H^+OH^-) or ZnNiO-(H^+OH^-) heterocluster shows that these heteroclusters could be the great semiconductor materials for many different uses.

Acknowledgments

In successfully completing this paper and its research, the authors are grateful to Kastamonu University.

Funding

This research received no funding.

Conflicts of Interest

The author declares no conflict of interest.

References

1. S.Z. Zainabidinov, A.Y. Boboev, M.B. Rasulova, N.Y. Yunusaliyev. X-ray diffraction analysis, optical characteristics and electro-physical properties of the N-ZnO/P-NiO structure grown by the spray pyrolysis method. New Materials, Compounds and Applications. 8(3), 2024, 411-421. https://doi.org/10.62476/nmca83411
2. S. Parmonov, K. Sharipov, D. Mirzavaliyev, F. Makhmudova, N. Askarova, R. Toshkodirova, N. Abdullaeva, M. Rifky, J.M. Harris, A. Kambarov. The technology of obtaining powders used in the production of solid alloys. New Materials, Compounds and Applications. 8(3), 2024, 450-458. https://doi.org/10.62476/nmca83450
3. Monajjemi, M., Mohammadi, S., Shahriari, S. *et al.* Experimental and Theoretical Studies of ZnO Nanotubes: an Approach to Chemical Physics Characterization of ZnONTs, Including Morphology, Piezoelectric, and Density of States. *Russ. J. Phys. Chem. B* 18, 308–324 (2024). https://doi.org/10.1134/S1990793124010342
4. Vasin, A.A., Dobryakov, A.L., Kochev, S.Y. *et al.* Relaxation of Multiple Excitons in ZnCdS and ZnCdS/ZnS Alloy Quantum Dots. *Russ. J. Phys. Chem. B* 18, 1646–1650 (2024). https://doi.org/10.1134/S1990793124701380
5. Olkhovskaya, I.P., Krokhmal, I.I. & Glushchenko, N.N. Improvement of the Morphophysiological Parameters of Pepper after the Presowing Treatment of Seeds with Zinc Nanoparticles. *Russ. J. Phys. Chem. B* 18, 527–532 (2024). https://doi.org/10.1134/S1990793124020295
6. I.I. Abbasov, M.A. Musayev, C.I. Huseynov, Q.Y. Eyyubov, N.N. Hasimova, A.J. Mammadova, A.A. Hadieva, Y.I. Aliyev, N.A. Qasumov, R.Sh. Rahimov. A study of impurity defect photoluminescence in ZnSe:Cr and ZnSe:Fe in the near infrared at room temperature. Advanced Physical Research. 5(3), 2023, 192-199
7. Zhang, X.Q., Zhang, B. Effect of Pressure on the Structural, Mechanical, and Electronic Properties of Monoclinic $ZnWO_4$. *Russ. J. Phys. Chem. B* 17, 1049–1056 (2023). https://doi.org/10.1134/S1990793123050135

8. Ikim, M.I., Spiridonova, E.Y., Gromov, V.F. *et al.* Effect of the Formation Method of ZnO–In_2O_3 Composites on Their Structural Characteristics and Conductivity. *Russ. J. Phys. Chem. B* 18, 283–288 (2024). https://doi.org/10.1134/S199079312401010X
9. Zverev, A.S., Zvekov, A.A., Pugachev, V.M. *et al.* Controlling the Sensitivity of Pentaerythritol Tetranitrate to Visible Laser Radiation by the Addition of ZnO:Ag Nanopowder. *Russ. J. Phys. Chem. B* 17, 1135–1142 (2023). https://doi.org/10.1134/S1990793123050147
10. Yuan, X., Tan, X. & Liu, B. Structural, Mechanical, Electronic and Optical Properties of Spinel $ZnAl_2O_4$ Underpressure from First-Principles Calculations. *Russ. J. Phys. Chem. B* 17, 886–895 (2023). https://doi.org/10.1134/S1990793123040322
11. Martin, O.; González, V.; Tirado, M.; Comedi, D. Effects of methanol on morphology and photoluminescence in solvothermal grown ZnO powders and ZnO on Si. *Mater. Lett.* 2019, *251*, 41–44.
12. Xiong, H.M.; Liu, D.P.; Xia, Y.Y.; Chen, J.S. Polyether-grafted ZnO Nanoparticles with Tunable and Stable Photoluminescence at Room Temperature. *Chem. Mater.* 2005, *17*, 3062–3064.
13. Agarwal, D.C.; Singh, U.B.; Gupta, S.; Singhal, R.; Kulriya, P.K.; Singh, F.; Tripathi, A.; Singh, J.; Joshi, U.S.; Avasthi, D.K. Enhanced room temperature ferromagnetism and green photoluminescence in Cu doped ZnO thin film synthesised by neutral beam sputtering. *Sci. Rep.* 2019, *9*, 6675.
14. Wolska, E.; Kaszewski, J.; Kiełbik, P.; Grzyb, J.; Godlewski, M.M.; Godlewski, M. Rare earth activated ZnO nanoparticles as biomarkers. *Opt. Mater.* 2014, *36*, 1655–1659
15. Lim, J.H.; Kang, C.K.; Kim, K.K.; Park, I.K.; Hwang, D.K.; Park, S.J. UV Electroluminescence Emission from ZnO Light-Emitting Diodes Grown by High-Temperature Radiofrequency Sputtering. *Adv. Mater.* 2006, *18*, 2720–2724.
16. Tolubayeva, D.B.; Gritsenko, L.V.; Kedruk, Y.Y.; Aitzhanov, M.B.; Nemkayeva, R.R.; Abdullin, K.A. Effect of Hydrogen Plasma Treatment on the Sensitivity of ZnO Based Electrochemical Non-Enzymatic Biosensor. *Biosensors* 2023, *13*, 793. https://doi.org/10.3390/bios13080793
17. Liu, H.; Zhang, Y.; Zhang, H.; Wang, L.; Wang, T.; Han, Z.; Wu, L.; Liu, G. Effect of plasma vitamin C levels on Parkinson's disease and age at onset: A Mendelian randomization study. *J. Transl. Med.* 2021, *19*, 221.
18. Abdullin, K.A.; Gabdullin, M.T.; Gritsenko, L.V.; Ismailov, D.V.; Kalkozova, Z.K.; Kumekov, S.E.; Mukash, Z.O.; Sazonov, A.Y.; Terukov, E.I. Electrical, Optical, and Photoluminescence Properties of ZnO Films Subjected to Thermal Annealing and Treatment in Hydrogen Plasma. *Semiconductors* 2016, *50*, 1010–1014.
19. Chang, S.-C.; Hu, J.-C.; Chan, H.-T.; Hsiao, C.-A. Influence of Processing Time in Hydrogen Plasma to Prepare Gallium and Aluminum Codoped Zinc Oxide Films for Low-Emissivity Glass. *Coatings* 2022, *12*, 945.
20. Chang, S.-C.; Li, T.-H.; Chan, H.-T. Hydrogen Plasma Annealed Titanium Dioxide Oxide/Aluminum-doped Zinc Oxide Films Applied in Low Emissivity. Glass. *Int. J. Electrochem. Sci.* 2021, *16*, 210817.
21. Zhang, C.; Cao, Z.; Zhang, G.; Yan, Y.; Yang, X.; Chang, J.; Song, Y.; Jia, Y.; Pan, P.; Mi, W.; et al. An electrochemical sensor based on plasma-treated zinc oxide nanoflowers for the simultaneous detection of dopamine and diclofenac sodium. *Microchem. J.* 2020, *158*, 105237.
22. Srijita NundyAritra Ghosh*Tapas K. Mallick, Hydrophilic and Superhydrophilic Self-Cleaning Coatings by Morphologically Varying ZnO Microstructures for Photovoltaic and Glazing Applications. ACS Omega 2020, 5, 2, 1033–1039. https://doi.org/10.1021/acsomega.9b02758
23. David Raymand, Adri C.T. van Duin, Daniel Spångberg, William A. Goddard III, Kersti Hermansson, Water adsorption on stepped ZnO surfaces from MD simulation, Surface Science, 604(9–10), 741–752 (2010). https://doi.org/10.1016/j.susc.2009.12.012
24. T. Dietl, Ferromagnetic semiconductors. Semicond. Sci.Technol. 17(4), 377–392 (2002)
25. P. Raji and K. Balachandra Kumar, Investigation of Ti doping on the structural, optical, and magnetic properties of ZnO nanoparticles. J Mater Sci: Mater Electron (2021) 32:11751–11762.

https://doi.org/10.1007/s10854-021-05803-y.
26. Q. Shao, C. Wang, J.A. Zapien, C.W. Leung, A. Ruotolo, Ferromagnetism in Ti-doped ZnO thin films. J. Appl. Phys. 117(17), 17B908 (2015)
27. H.S. Lokesha, A.R.E. Prinsloo, P. Mohanty, C.J. Sheppard, Impact of Cr doping on the structure, optical and magnetic properties of nanocrystalline ZnO particles. *Journal of Alloys and Compounds.* 960, 2023, 170815. https://doi.org/10.1016/j.jallcom.2023.170815
28. Antwi, R. A., Nkrumah, I., Ampong, F. K., Paal, M., Tamakloe, R. Y., Nkum, R. K., & Boakye, F. (2023). Synthesis of Pure and Manganese Doped Zinc Oxide Nanoparticles by a Solution Growth Technique: Structural and Optical Investigation. East European Journal of Physics, 4, 129-136 (2023). https://doi.org/10.26565/2312-4334-2023-4-13
29. Anindita Samanta, M.N. Goswami, P.K. Mahapatra, Nickel doped ZnO nanoparticles as a novel photocatalytic and multiferroic semiconductor. *Physica E: Low-dimensional Systems and Nanostructures*. 158, 115885 (2024). https://doi.org/10.1016/j.physe.2023.115885
30. W. Kohn, L. J. Sham, Self-Consistent Equations Including Exchange and Correlation Effects. *Phys. Rev*., 140, A1133–A1138 (1965). https://doi.org/10.1103/PhysRev.140.A1133
31. A.D. Becke, Density-functional thermochemistry. III. The role of exact exchange. *J Chem Phys* 98(7), 5648–5652 (1993). https://doi.org/10.1063/1.464913
32. C. Lee, W. Yang, R.G. Parr, Development of the Colle–Salvetti correlation-energy formula into a functional of the electron density. *Phys Rev B*. 37, 785–789 (1988). https://doi.org/10.1103/PhysRevB.37.785
33. J.P. Perdew, K. Burke, M. Ernzerhof, Generalized Gradient Approximation Made Simple. *Phys. Rev. Lett.* 77, 3865 (1996). https://doi.org/10.1103/PhysRevLett.77.3865
34. Mollaamin, F. Anchoring of 2D layered materials of $Ge_5Si_5O_{20}$ for (Li/Na/K)-(Rb/Cs) batteries towards Eco-friendly energy storage. *BMC Chemistry* 19, 233 (2025). https://doi.org/10.1186/s13065-025-01593-0
35. Jianwei Sun, James W. Furness, Yubo Zhang, Chapter 4 - Density functional theory. *Mathematical Physics in Theoretical Chemistry*. *Developments in Physical & Theoretical Chemistry.* 2019, 119-159. https://doi.org/10.1016/B978-0-12-813651-5.00004-8
36. Arrigoni, M.; Madsen, G.K.H. Comparing the performance of LDA and GGA functionals in predicting the T lattice thermal conductivity of III-V semiconductor materials in the zincblende structure: The cases of AlAs and BAs. Comput. Mater. Sci. 2019, 156, 354–360.
37. Mollaamin, F. Efficiency Probing of GaInP/GaInAs-Based Solar Cells through Synergy of Silicon, Zinc or Silver Elements: A First-Priciples Study. *Russ. J. Phys. Chem. B* 19, 1222–1238 (2025). https://doi.org/10.1134/S1990793125700915
38. Frisch, M. J.; Trucks, G. W.; Schlegel, H. B.; Scuseria, G. E.; Robb, M. A.; et al. Gaussian 16, Revision C.01, Gaussian, Inc., Wallingford CT, 2016.
39. GaussView, Version 6.06.16, Dennington, Roy; Keith, Todd A.; Millam, John M. Semichem Inc., Shawnee Mission, KS, 2016.
40. Zihan Xu, Chenglong Qin, Yushu Yu, Gang Jiang, Liang Zhao, First-principles study of adsorption, dissociation, and diffusion of hydrogen on α-U (110) surface. AIP Advances 14, 055114 (2024). https://doi.org/10.1063/5.0208082.
41. Lu, T.; Chen, F. Multiwfn: A multifunctional wavefunction analyzer. *J. Comput. Chem.* 2012, *33*, 580–592. https://doi.org/10.1002/jcc.22885.
42. Lu, T. A comprehensive electron wavefunction analysis toolbox for chemists, Multiwfn. *J. Chem. Phys.* 2024, *161*, 082503. https://doi.org/10.1063/5.0216272.
43. H.L Schmider, A.D Becke, Chemical content of the kinetic energy density. Journal of Molecular Structure: THEOCHEM. 527(1–3), 51-61 (2000). https://doi.org/10.1016/S0166-1280(00)00477-2.
44. V. Tsirelson and A. Stash, Analyzing experimental electron density with the localized-orbital locator. Acta Cryst. B58, 780-785 (2002). https://doi.org/10.1107/S0108768102012338